Evaluation of IMERG Satellite Precipitation over the Land–Coast–Ocean Continuum. Part II: Quantification

YAGMUR DERIN,[a] PIERRE-EMMANUEL KIRSTETTER,[a,b,c] NOAH BRAUER,[a,b] JONATHAN J. GOURLEY,[c] AND JIANXIN WANG[d,e]

[a] *Advanced Radar Research Centerand School of Civil Engineering and Environmental Sciences, University of Oklahoma, Norman, Oklahoma*
[b] *School of Meteorology, University of Oklahoma, Norman, Oklahoma*
[c] *NOAA/National Severe Storms Laboratory, Norman, Oklahoma*
[d] *Science System Applications, Inc., Lanham, Maryland*
[e] *NASA Goddard Space Flight Center, Greenbelt, Maryland*

(Manuscript received 1 December 2021, in final form 27 April 2022)

ABSTRACT: To understand and manage water systems under a changing climate and meet an increasing demand for water, a quantitative understanding of precipitation is most important in coastal regions. The capabilities of the Integrated Multi-satellitE Retrievals for Global Precipitation Measurement (IMERG) V06B product for precipitation quantification are examined over three coastal regions of the United States: the West Coast, the Gulf of Mexico, and the East Coast, all of which are characterized by different topographies and precipitation climatologies. A novel uncertainty analysis of IMERG is proposed that considers environmental and physical parameters such as elevation and distance to the coastline. The IMERG performance is traced back to its components, i.e., passive microwave (PMW), infrared (IR), and morphing-based estimates. The analysis is performed using high-resolution, high-quality Ground Validation Multi-Radar/Multi-Sensor (GV-MRMS) rainfall estimates as ground reference at the native resolution of IMERG of 30 min and 0.1°. IMERG Final (IM-F) quantification performance heavily depends on the respective contribution of PMW, IR, and morph components. IM-F and its components overestimate the contribution of light rainfall (<1 mm h^{-1}) and underestimate the contribution of high rainfall rates (>10 mm h^{-1}) to the total rainfall volume. Strong regional dependencies are highlighted, especially over the West Coast, where the proximity of complex terrain to the coastline challenges precipitation estimates. Other major drivers are the distance from the coastline, elevation, and precipitation types, especially over the land and coast surface types, that highlight the impact of precipitation regimes.

KEYWORDS: Atmosphere; Coastlines; Complex terrain; Coastal meteorology; Hydrometeorology; Orographic effects; Radars/Radar observations; Remote sensing; Satellite observations

1. Introduction

Coasts form a narrow zone between land and ocean that host large and growing human population, economic activity, and diverse plant and animal species. Eight of the top 10 largest cities in the world are in coastal areas. Most importantly, coastal regions and populations are exposed to hazards from both land and ocean. Rappaport (2014) reports that in a 50-yr period (1963–2012) around 2544 people died of coastal water from tropical cyclones in the United States. In 2017, category 4 storm Hurricane Harvey hit Texas and caused $125 billion in damage (National Weather Service 2018). In 2020, category 5 storm Typhoon Goni hit the Philippines and Vietnam and caused $392 million of damage and was responsible for approximately 74 deaths. This typhoon lasted for 54 h and was considered to be the strongest landfalling tropical cyclone to ever be recorded. Precipitation plays an important role in the monitoring, analysis, and planning of water-related disasters (e.g., flood and drought; Yilmaz et al. 2005; Nalbantis 2008). Hence, accurate precipitation measurement and estimation over coastal regions is critical. However, there are challenges in precipitation measurement and estimation due to extreme spatiotemporal variability.

Precipitation can be measured using in situ observations or remote sensors. In situ sensors (e.g., rain gauges and disdrometers) provide direct precipitation measurements, but their coverage is limited due to the local nature of these measurements and uneven availability especially over coasts, oceans, and complex terrain. A detailed understanding and observation of precipitation over the land–coast–ocean continuum can only be achieved with remote sensors (e.g., ground radars

Corresponding author: Pierre-Emmanuel Kirstetter, pierre.kirstetter@noaa.gov

DOI: 10.1175/JHM-D-21-0234.1

or satellite sensors). Remote sensors can depict precipitation amount, frequency, and distribution at fine spatiotemporal scale (Huffman et al. 2020).

Satellite-based precipitation products (SPPs) provide the best spatial and temporal coverage on the global scale, especially over the land–coast–ocean continuum. The great success of the Tropical Rainfall Measuring Mission (TRMM) has led to the Global Precipitation Measurement Mission (GPM) and accelerated the development of new SPP algorithms, such as the Integrated Multi-satellitE Retrievals for Global Precipitation Measurement (IMERG). To obtain high spatiotemporal resolution (0.1°, 30 min) and global coverage, IMERG merges available Level-2 passive microwave (PMW) and infrared (IR) precipitation retrievals (Huffman et al. 2020). Hence, sources of uncertainty that affect the detection or quantification of precipitation in IMERG can arise from either the satellite sensors or algorithms for estimating rainfall (Tan et al. 2016; Gebregiorgis et al. 2017, 2018; Kirstetter et al. 2020). Multiple uncertainties are associated with Level-2 PMW, and IR precipitation retrievals and Level-3 merged SPPs, especially in coastal regions. Precipitation retrievals from PMW observations highly depend on the ability to separate emission and scattering radiances of rain, ice, and clouds from Earth's surface (e.g., Kummerow and Giglio 1994; Carr et al. 2015; Turk et al. 2021). This is a complicated task and while the ocean surface is radiometrically cold and homogeneous, the land surface is warm and heterogeneous. Coastal regions include contrasting radiative contributions from both ocean and land hence yielding one of the most uncertain precipitation retrievals. It should be noted that the GPM-era retrievals have not been evaluated over the land–coast–ocean continuum. A few studies investigate the IMERG performance in the coastal regions. Sui et al. (2020) identified heterogenous errors in PMW and IR estimates over coastal regions of Southeast China. Wang et al. (2019) reported that IMERG underestimated precipitation over coastal regions in Guangdong Province, China and showed that this is due to missed precipitation and negative hit bias. Both the GPM Ground Validation (GV) team and IMERG algorithm developers highlight the importance of evaluation studies in "nontraditional" regions such as coasts and ocean.

The companion manuscript to this paper (Derin et al. 2021, hereafter Part I) introduced the study domain, surface type classification, radar–rain gauge corrected precipitation reference, and IMERG products and matchup methodology. IMERGV06B Final, Late, and Early and the abilities of their PMW and IR components to detect precipitation over the land–coast–ocean continuum were examined and linked to surface and precipitation characteristics over the United States. In this study, IMERG and its components quantification performance over the land–coast–ocean continuum over CONUS is examined. To address the transferability of regional evaluation results to different geographical regions, three different coastal regions of the CONUS are considered, namely, the West Coast, the Gulf of Mexico, and the East Coast.

The West Coast is characterized by mountain peaks and steep slopes adjacent to the coastline. Moist airflow that encounters these slopes is lifted, cooled, and produces orographic rainfall. During the winter season, synoptic-scale cyclones and fronts from the Pacific Ocean undergo complex interactions with coastal mountains within 50 km of the coastline. This upslope flow mechanism is a relatively simple conceptual model that can explain the significant fraction of orographic rainfall observed over the West Coast (Roe 2005; Houze 2012). Orographic mechanisms tend to generate low-level enhancement of precipitation with lower ice content aloft (Purnell and Kirshbaum 2018). It leaves tenuous signatures in the observed satellite brightness temperatures. PMW retrievals rely on ice content aloft over land and IR retrievals rely on cold cloud top temperature to infer precipitation, hence PMW and IR retrievals tend to underestimate these events. On the other hand, the Gulf Coast is characterized by flat terrain. During the warm season, sea-breeze fronts, convective storms, and tropical cyclones are observed, while during the cool season the Gulf coast is dominated by the return flow of Gulf-modified warm, moist air and cold front passages. The East Coast is characterized by the Appalachian Mountains and complex coastal features consisting of barrier islands and coastal inlets. During the warm season, the Gulf Stream induces significantly different conditions from the land in terms of wind, humidity, and temperature. During the cool season, offshore Gulf Stream frontal features are combined with cold air over land, producing complex mesoscale cloud systems. These mesoscale ocean features include intense coastal cyclogenesis, which often brings freezing rain, sleet, and snow from North Carolina through New England (Young and Sikora 2003).

Precipitation mechanisms are complex and depend on several environmental and physical parameters. Hence, considering environmental and/or physical parameters to condition matchup dataset (reference dataset and SPP) could provide more detailed analysis of SPP performance. In this manuscript, the ability of the IMERG products to quantify precipitation over the land–coast–ocean continuum is examined at the IMERG native resolution (30 min and 0.1°), and linked to distance to coastline, surface, and precipitation characteristics over the United States.

This paper is organized as follows. The dataset and evaluation method are represented in section 2. Section 3 discusses the results, and section 4 summarizes our findings and offers recommendations for future research directions.

2. Datasets and evaluation method

a. GV-MRMS

The ground-based, radar–rain gauge corrected, 1-km spatial and 2-min temporal resolution GV-MRMS is used as a reference dataset (Kirstetter et al. 2012, 2018). GV-MRMS provides a radar quality index (RQI) to represent the level of uncertainty associated with reflectivity changes with height and near the melting layer. RQI ranges from 0 (worst) to 100 (best) (Zhang et al. 2011). A high quality and standardized reference are obtained by removing lower RQI estimates. Additional gauge-based corrections, quality and quantity controls, and resampling procedures are applied and described in detail in Kirstetter et al. (2012, 2014, 2015). In

this study, the radar–gauge-based GV-MRMS is used over a period of 12 months in 2015.

b. IMERG algorithm

IMERG is a Level-3 merged SPP. The IMERG algorithm intercalibrates, merges, and interpolates all available microwave retrievals, microwave-calibrated IR satellite estimates, and rain gauge measurements. Since low-Earth-orbiting PMW observations are too sparse, IMERG merges PMW and IR when necessary to output a high temporal resolution dataset. This happens in two ways: (i) PMW data are morphed using quasi Lagrangian time interpolation and estimated precipitation feature motion and (ii) IR estimates are merged with PMW using a Kalman filter (morph+IR) when PMW estimates are too sparse.

Even though IMERG provides high spatial and temporal global coverage, it is associated with multiple uncertainties in coastal regions. These uncertainties can be traced back to the merging components of Level-2 PMW and IR precipitation retrievals. Moreover, uncertainties in these Level-2 products arise from different mechanisms. Precipitation retrievals from PMW observations highly depend on the ability to separate emission and scattering radiances of rain, ice, and clouds from Earth's surface (Kummerow 2020). Low surface emissivity from the ocean creates a strong contrast between a radiometrically cold background and warm, precipitation-related atmospheric signature (Kummerow et al. 2001). On the other hand, land surfaces are highly emissive, which leads to similar brightness temperature emission signatures with rain. Hence, rainfall detection over land is based primarily on ice-induced scattering signatures (Wang et al. 2009). Precipitation retrieval over the coast becomes a complicated task since the ocean surface is radiometrically cold and homogenous, while the land surface is warm and heterogeneous. On the other hand, precipitation retrievals from IR observations are indirect (Kirstetter et al. 2018), and the primary idea is to infer precipitation occurrence and intensity at the surface from cloud-top temperatures.

In this study, IMERG version 06B Early, Late, and Final (IM-E, IM-L, and IM-F, precipitationCal fields) are evaluated with the aim of understanding the performance of each run, PMW and IR components, specifically the morphing, and the effectiveness of rain gauge correction over the land–coast–ocean continuum. To track uncertainties from Level-2 algorithms, IMERG-PMW (PMW) and IMERG-IR (IR) precipitation estimates are examined using ancillary variables provided by IMERG. The HQprecipitation and IRprecipitation fields are used for PMW and IR, respectively. The new PMW morphing procedure (morph) is targeted by selecting instances from precipitationUncal field where there is no PMW retrieval (HQprecipSource reports zero) and no IR contributed estimate (IRkalmanFilterWeight of 0%). IRkalmanFilterWeight between 0% and 100% corresponds to a mixture of morphed PMW and IR estimates (morph+IR) from precipitationUncal field.

c. Surface type classification

To ensure consistency with IMERG, surface type classification is extracted from the GMI GPROF-V05 surface type dataset. The GMI GPROF-V05 classification is derived by the Colorado State University surface classification scheme (GPROF-V05; Huffman et al. 2019). It classifies 10 land classes using self-similar mean emissivity from all available SSM/I observations (1993–2008, Prigent et al. 1997), to which ocean, sea ice, and two different boundaries that are possible in between land–ocean, and ocean–sea ice surface types are added. In this study, three surface types are used, namely, land, ocean, and coast.

d. Data matchup

GV-MRMS and IMERG matchups are extracted following a temporal and spatial matching at IMERG native resolution. The analysis is conducted at IMERG native resolution so that the results remain free of undesirable impacts caused by statistical or dynamical resampling (Kirstetter et al. 2012, 2015). To conduct a fair analysis and ensure high-quality radar observations, matchup datasets that are within 100 km from the closest NEXRAD are chosen. GV-MRMS rain/no rain threshold is set as 0.1 mm h^{-1} and matchup datasets that have RQI of 100 (i.e., best possible quality) are used. Moreover, GV-MRMS provides precipitation types for each grid cell. Note that cells reporting snow are disregarded from this analysis. The minimum detectable rain rate from the Ka- and Ku-band radar are 0.2 and 0.5 mm h^{-1}, respectively (Hou et al. 2014). GPROF is calibrated by these radar-based products, yet the IMERG estimate could produce rain rates lower than these two thresholds due to the inclusion of data from other sensors. Thus, the IMERG rain/no rain threshold is set at 0.1 mm h^{-1}.

As mentioned previously, the comparison dataset is divided into three different surface types as land, coast, and ocean and three different coastal regions as the West Coast, Gulf of Mexico, and East Coast.

e. Evaluation method

The evaluation of IMERG is conducted in two major steps defined as detection (Part I) and the quantification analysis, which is the focus of this manuscript. Several common validation statistics are employed to characterize differences between the retrieved estimates and the reference (GV-MRMS) values, such as the mean relative error (MRE), the linear correlation coefficient (CORR), and the centralized root-mean-square error (CRMSE). It bears emphasizing that bulk statistical scores provide overall information regarding the agreement of the SPP relative to the validation dataset, which in return invariably depends on the statistical and physical properties of the validation dataset. The overall information extracted from bulk statistics does not pinpoint SPPs' sources of uncertainties. Precipitation mechanisms are complex and depend on several environmental and physical parameters. Hence, considering environmental and/or physical parameters to condition the matchup dataset provides a basis for more detailed uncertainty analyses of SPPs. In this study, MRE, CRMSE and CORR are analyzed with respect to the distance to coastline, and elevation. Conditioning the matchup dataset with these physical parameters aim at capturing trends characterizing sources of uncertainty in SPPs. Similarly, IMERG is broken down into its components as PMW, IR, morph, and morph+IR so that the uncertainty can also be tracked backed

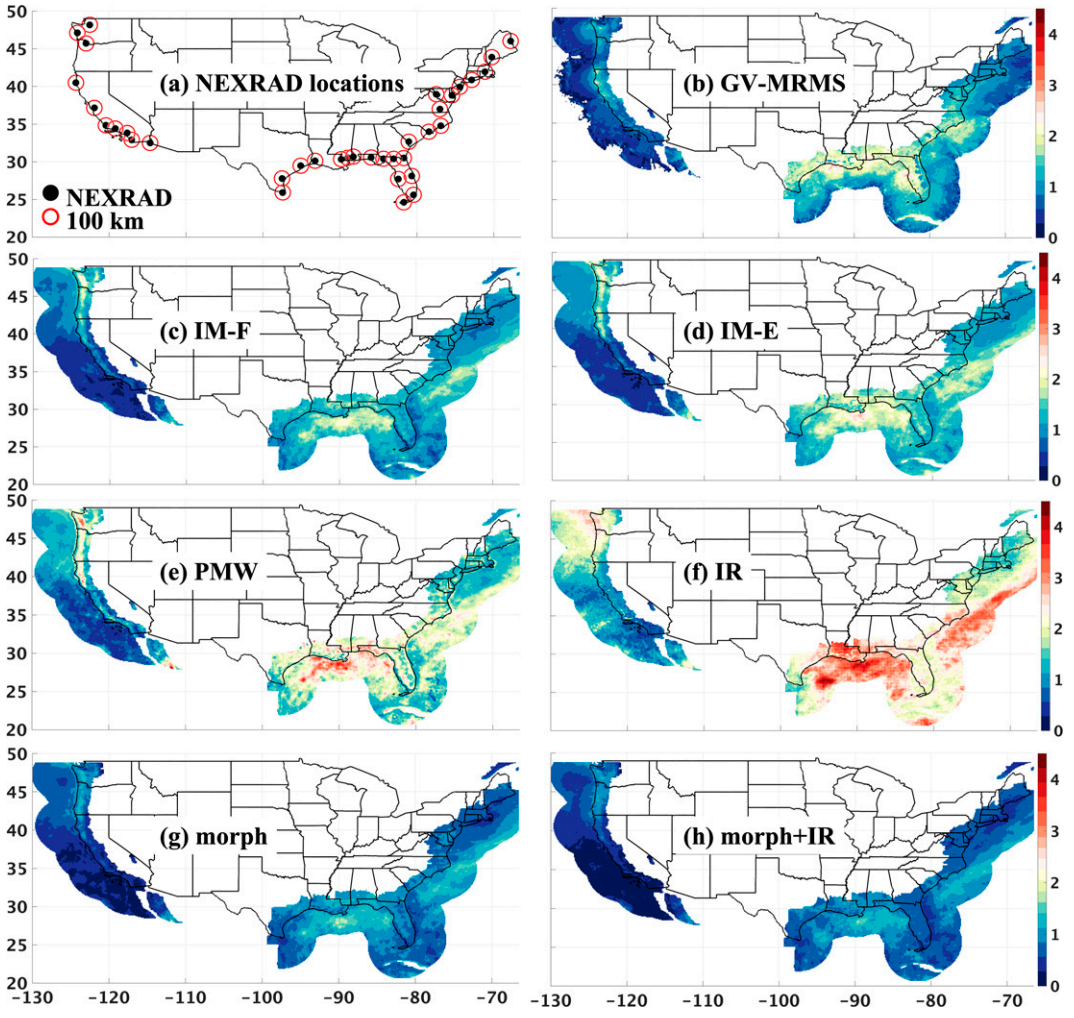

FIG. 1. Conditional mean rainfall during year 2015 for (b) GV-MRMS, (c) IM-F, (d) IM-E, (e) PMW, (f) IR, (g) morph, and (h) morph+IR and (a) NEXRAD locations over CONUS.

to Level-2 retrievals. Other statistics used to evaluate IMERG involve (i) spatial maps, (ii) probability of occurrence and volume, and (iii) bivariate histograms.

Each of the above is undertaken separately for each surface type (land, coast, and ocean) and region (West, East, and Gulf Coasts of CONUS). The evaluation is conducted by conditioning the dataset based on distance from coastline, elevation, rainfall magnitude, and rainfall type.

The MRE quantifies the degree of systematic component of the uncertainty, normalized by the mean rain rate of the GV-MRMS. CRMSE is a measure of the random component of the error since bias has been removed:

$$\mathrm{MRE} = \frac{\sum(\mathrm{SPP} - \mathrm{GV})}{\sum \mathrm{GV}}, \tag{1}$$

$$\mathrm{CRMSE} = \frac{\sqrt{\frac{1}{M}\sum\left[\mathrm{SPP} - \mathrm{GV} - \frac{1}{M}\sum(\mathrm{SPP} - \mathrm{GV})\right]^2}}{\frac{1}{M}\sum \mathrm{GV}}, \tag{2}$$

where GV represents GV-MRMS, and SPP represents IMERG, or its components rainfall magnitudes. CORR is an indicator of the temporal and spatial linear similarities between SPP and GV-MRMS. Perfect MRE is zero (no bias), positive MRE indicates that SPP is overestimating, and negative MRE indicates that SPP is underestimating.

3. Rainfall quantification results

a. General performance

The climatology of precipitation varies significantly across the United States. Their depiction varies also with precipitation products. To understand this variability and the satellite rainfall retrieval performances with respect to the reference over the ocean, coast, and land surfaces, Fig. 1 represents GV-MRMS, IM-F, IM-E, PMW, IR, morph, and morph+IR conditional mean (>0.1 mm h^{-1}) rainfall for the year 2015. To evaluate discrepancies between SPP and GV-MRMS when it rains, conditional mean rainfall is used here instead of unconditional

mean rainfall. Only cases where precipitation is detected either by SPP or GV-MRMS are considered. Figure 1b shows that GV-MRMS conditional mean rainfall decreases further away from the coast at distances beyond 100 km from the radar sites. This is related to radar sampling conditions that deteriorate with distance (i.e., radar beamwidth and height), which is clearly indicated in the RQI distribution (Wang et al. 2021). As mentioned in the previous section, to ensure a high-quality ground reference, GV-MRMS data within 100 km of NEXRAD locations (black dots represents each reporting NEXRAD locations and red circles represent the 100 km diameter around each NEXRAD in Fig. 1a) are considered in this study. While it only partly represents open ocean rainfall conditions, it provides good representation of the land, coast, and ocean continuum.

GV-MRMS (Fig. 1b) observes the highest conditional mean rainfall over the Gulf Coast compared to the West and East Coasts. It is related to the tropical cyclone activity that affects this region. The spatial distribution is captured by all IMERG products, with uncertainty in terms of magnitude. IM-F (Fig. 1c) and IM-L (not shown here) performances are very similar to each other and closest to the GV-MRMS ground reference visually. It should be noted here that IM-L and IM-E products are satellite only meanwhile IM-F is gauge corrected. This suggests that the monthly gauge correction does not influence the quantity of precipitation across IM-L and IM-F. This could be due to lack of reporting rain gauges in the land-coast-ocean continuum. IM-E (Fig. 1d) shows overestimation compared to GV-MRMS, IM-F, and IM-L. Part I of this study showed the benefits of backward- and forward-propagated PMW estimates (morph) used in IM-L and IM-F compared to forward-propagated PMW estimates used in IM-E because the forward-propagated PMW estimates generates higher detection rates and lower miss rates. IM-E overestimation could be an indication of the limitation associated with the forward-only propagated PMW estimates. Looking at the IMERG components, PMW (Fig. 1e) shows overestimation over the Gulf Coast and the Northwest coastline. As expected, morph (Fig. 1g) shows a similar spatial distribution compared to PMW but with significantly lower conditional mean rainfall. This could be due to smoothing effects of forward- and backward-propagation techniques applied on PMW estimates to calculate morph dataset. Hence, even though the spatial distribution of PMW is maintained, the conditional mean rainfall is significantly decreased. Regarding the IR component, Part I highlighted IR-based rainfall detection challenges, especially missed precipitation where IR conditional relative rainfall occurrence is reported to be generally lower than 50% (30%) over the East Coast (Northwest coast). Here, IR displays the highest overestimation compared to GV-MRMS, which indicates that quantification is also a challenge with the IR-based retrievals. Over the West Coast, while PMW (Fig. 1e) captures the orographic enhancement causing the gradual increase inland, IR (Fig. 1f) reports overestimation over ocean, coast, and land and does not capture the spatial distribution of precipitation over this region. PMW displays similar geospatial features as GV-MRMS over Gulf Coast, yet with slight overestimation. Meanwhile, IR does not capture the spatial distribution and reports significant overestimation over the Gulf Coast. On the other hand, morph+IR (Fig. 1h) reports the lowest conditional mean rainfall compared to all other products. This suggests that the main contributor in morph+IR is morph; however, it is surprising that the morph+IR conditional mean rainfall is lower than morph as well. This could be because the weights used in the Kalman filter scheme decrease and smooth the conditional mean rainfall while merging IR and morph.

As mentioned in section 2, IMERG product's Level-2 components PMW, IR, morph, and morph+IR precipitation estimates are examined individually to track uncertainties from Level-2 algorithms. The contribution of each of the Level-2 datasets is shown in Fig. 2 with the percentage occurrence of PMW, IR-only, morph, and morph+IR in IM-F. For this figure only, IR-only instances are obtained from the precipitationUncal field with no PMW retrieval contribution (HQprecipSource reports zero) and with IRkalmanFilterWeight contribution equal to 100%. The IR-only contribution to the Level-3 IMERG product is lower than other components (<20%) and it is located on the East Coast and the Northwest coast (Fig. 2b). Due to performance issues of IR products, the IMERG algorithm minimizes the contribution of the IR-only precipitation retrievals. Meanwhile, PMW percentage of occurrence contribution is at around 20%–30% over all three regions (Fig. 2a). Overall PMW occurrence contribution is slightly higher over the Northwest and Northeast land–coast–ocean continuum. Even though PMW precipitation retrievals have comparatively better performance than other Level-2 products, their occurrence contribution is lower due to the sampling of low-Earth-orbiting satellites. Morph (Fig. 2c) has the higher percentage of occurrence (30%–50%) over the Northwest and Northeast CONUS compared to PMW. Morph was used slightly less over the Northeast land regions compared to ocean over the same region, meanwhile over the Gulf Coast, morph is used more frequently over the land surface type compared to ocean surface type. Part I reported that due to a lack of direct observations, the morphed PMW detection performance is lower (lower hits and higher false alarm rates) compared to PMW. The morphing increases the occurrence of estimated rainfall as indicated by higher percentage occurrence (Fig. 2c). Over the Gulf Coast, the Southeast, and the Southwest, morph+IR has the highest percentage of occurrence (50%–60%). Meanwhile, over the Northeast land and Northwest land and ocean, morph+IR has the lowest percentage of occurrence. Part I reported an overall trend of decreasing detection performance from PMW to morph to morph+IR and to IR products, with continuously decreasing hits and increasing false alarm rates. This trend highlights a tendency to overestimate rainfall occurrence with increasing time lag from PMW observations.

Figures 1 and 2 show that each IMERG products' performance depends on location because (i) rainfall characteristics and their spatial distributions vary significantly with climatology across the United States and (ii) the IMERG components have spatially uneven contributions to the merged product.

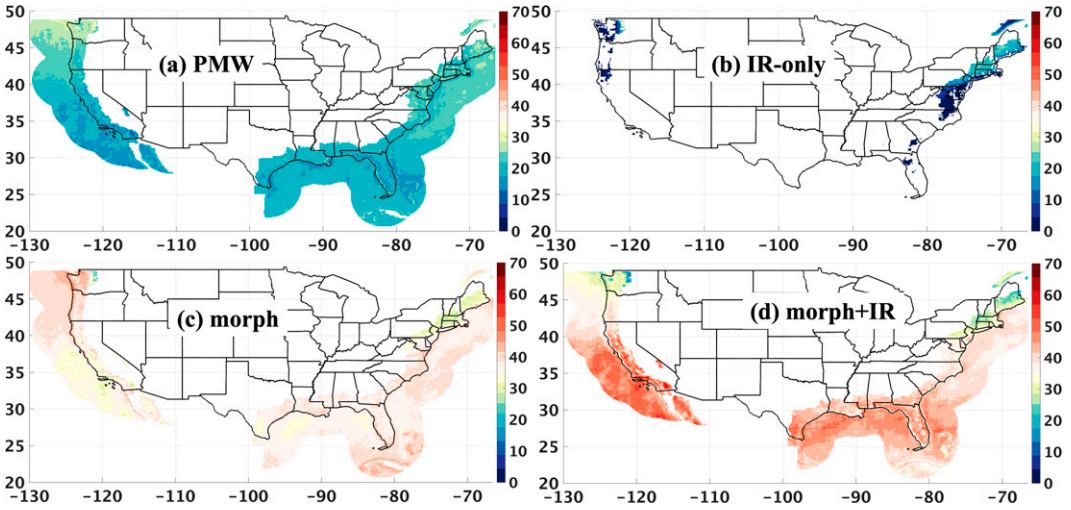

FIG. 2. Percentage of occurrence for (a) PMW, (b) IR-only, (c) morph, and (d) morph+IR. The percentage of each grid box is computed by dividing the number of samples of individual sensor by the total number of observations during the study period, hence for each pixel the added proportions make up to 100%.

In Figs. 3 and 4, PDF by occurrence (PDF_c) and by volume (PDF_v) of the 30-min rain rates are computed for each IMERG product and GV-MRMS, respectively. PDF_c displays the frequency of occurrences of each rain rate category to the total number of occurrences. PDF_v is the relative contribution of each rain rate bin to the total rainfall volume, computed as a ratio between the sum of the rain rates in each bin to the total sum of the rain rates (Wolff and Fisher 2008). PDF_c highlights the differences in GV-MRMS and SPP estimates' sensitivity as a function of rain rate. PDF_v highlights the influence of various rain rate magnitudes. Figure 3 represents PDF_c for each region and surface type for GV-MRMS (gray bars), and all SPPs (lines for each IMERG product and component). In terms of regional differences, GV-MRMS shows clear differences between the West Coast, Gulf Coast, and East Coast. Over the West Coast, the GV-MRMS distribution is narrower compared to other regions and it displays lower occurrence of higher rainfall. The distribution mode is around ~2.2 mm h^{-1} and skewed slightly to the left. Light to medium rainfall (0.1–2 mm h^{-1}) occurrence is highest compared to other regions. Over the Gulf Coast, GV-MRMS shows a wider distribution where occurrence of each rainfall rate is more uniformly distributed compared to other regions. Over the East Coast GV-MRMS distribution mode is around ~1.7 mm h^{-1} and skewed to the left. In terms of surface differences, GV-MRMS distribution display slightly lower rain rates over ocean compared to the land and coastal surface types over all regions.

Overall, in Fig. 3, SPPs have similar distributions by occurrence (mean [1.8–3.8 mm h^{-1}], standard deviation [1.7–5.3]) compared to the GV-MRMS distributions (mean [1.8–3.5 mm h^{-1}], standard deviation [1.7–5.3]) over all regions and surface types except IR (mean [2.1–4.1 mm h^{-1}], standard deviation [1.9–5.9]). The IR distribution is shifted toward higher rainfall rates especially over ocean. The IMERG components (PMW, morph+IR and morph) distributions are like each other and close to GV-MRMS distributions. Over the West Coast and consistently with GV-MRMS, all SPPs display narrower distributions than other regions (especially over ocean) with mode around ~2 mm h^{-1}, and a slight left skew. Over the Gulf Coast and the East Coast, SPPs (except IR) also display distributions consistent with GV-MRMS.

As GV-MRMS, most SPPs distributions do not show significant dependency with surface types (except IR) overall, but lighter precipitation rates are noted over the ocean.

Over the West Coast the GV-MRMS mode is at around 3.4 mm h^{-1} (Fig. 4). Most of the rainfall volume that falls over this region is in the range [1–5 mm h^{-1}]. Over the Gulf Coast, the GV-MRMS distribution is skewed to the left (mode ~7 mm h^{-1}) and the contribution of light rainfall to the total rainfall volume is minimum (mean ~10.5 mm h^{-1}). Over the East Coast, the mode of the GV-MRMS distribution is around ~4.5 mm h^{-1} and has a slight left skew. GV-MRMS PDF_v are very similar to each other over coast and land for all regions, yet it shows slight differences over ocean. GV-MRMS land and coast PDF_v distributions are similar but show regional differences with mean ~4.1 mm h^{-1} (~11.0 mm h^{-1}) and the standard deviation ~3.8 (~10.0) over the West (Gulf) Coast. Meanwhile, GV-MRMS PDF_v mean is 3.4 mm h^{-1} (6.7 mm h^{-1}) and standard deviation is 2.9 (8.5) over the ocean West (Gulf) Coast.

SPPs PDF_v shows systematic characteristics and departures with respect to the GV-MRMS PDF_v reference. SPPs PDF_v overestimate the contribution of light rainfall (<1 mm h^{-1}) and underestimate the contribution of high rainfall rates (>3 mm h^{-1}) to the total rainfall volume over all regions and surface types. It suggests the IMERG, and its components meet challenges with extreme precipitation events. Note that SPPs show more similar distribution curves with each other than with GV-MRMS including the IR PDF_v. Each region has distinct PDF_v characteristics and all SPPs capture these characteristics to some extent compared to

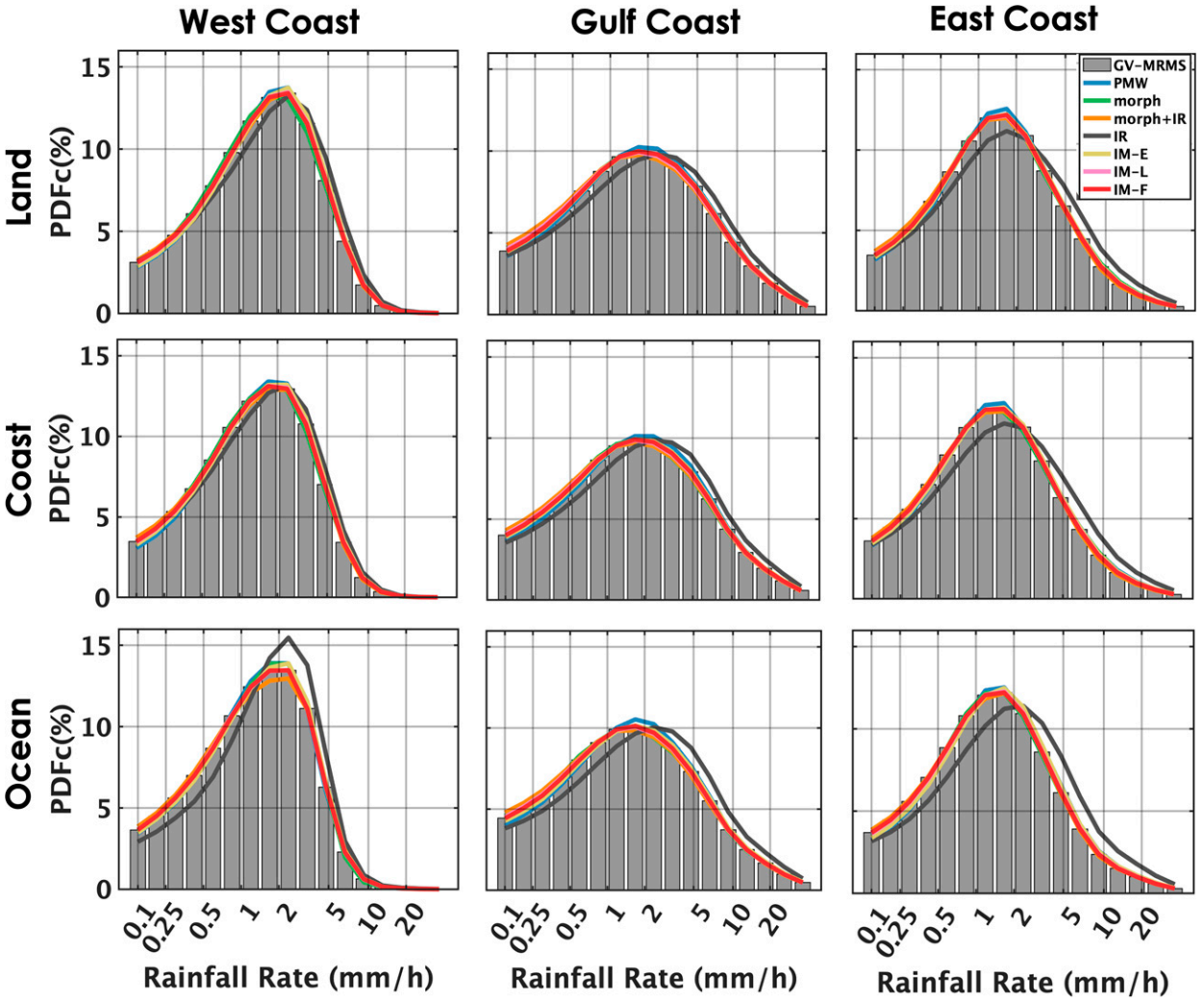

FIG. 3. PDF by occurrence (PDF_c) as a function of GV-MRMS rainfall rate (mm h^{-1}) over the (left) West Coast, (center) Gulf Coast, and (right) East Coast regions and (top) land, (middle) coast, and (bottom) ocean surface types.

GV-MRMS. Over the West Coast, all SPP distributions overestimate rainfall contributions up to ~1.5 mm h^{-1} and underestimate the contributions of heavier rainfall rates. IR performance is more similar to other products over ocean than over coast and land. Over the Gulf Coast, SPPs do not capture the features of GV-MRMS PDF_v as much. Specifically, the GV-MRMS PDF_v shows a left skewed distribution suggesting that light rain rates have less influence in this region dominated by tropical activity. SPPs do not capture this left skewed distribution and show more symmetrical distributions compared to GV-MRMS. Over the East Coast, the GV-MRMS distribution is also left skewed albeit slightly less than over the Gulf Coast, and SPPs do not capture the GV-MRMS PDF_v features contrasting the contributions of light versus heavy rainfall.

A general quantification evaluation of the SPP can be provided with density scatterplots of SPP with respect to GV-MRMS. Due to limited space, only IM-F is provided in Fig. 5 along with MRE, CRMSE, and CORR score values. Overall, IM-F quantification of light rainfall is poorer compared to medium and heavy rainfall. Over all surfaces and regions, IM-F slightly overestimates precipitation rates with MRE in the range from [−0.01 to +0.36], CORR around 0.5, while CRMSE values are quite high [2.9–4.5] relative to GV-MRMS.

The performance of IM-F varies slightly from region to region. Lowest (highest) MRE values are reported over the East Coast [0.01–0.26] (West Coast [0.24–0.36]). Meanwhile, lowest (highest) CRMSE values are reported over the West Coast [2.9–3.7] (Gulf Coast [3.1–4.5]), respectively. The IM-F overestimation over the West Coast occurs with higher rainfall magnitudes. The higher CRMSE values over the Gulf Coast are associated with lower densities along the 1:1 line. It indicates that IM-F quantification is challenged over this region. This could be due to extreme events (e.g., tropical cyclones) observed in this region, and this higher random component of the error could be due to either sensors or

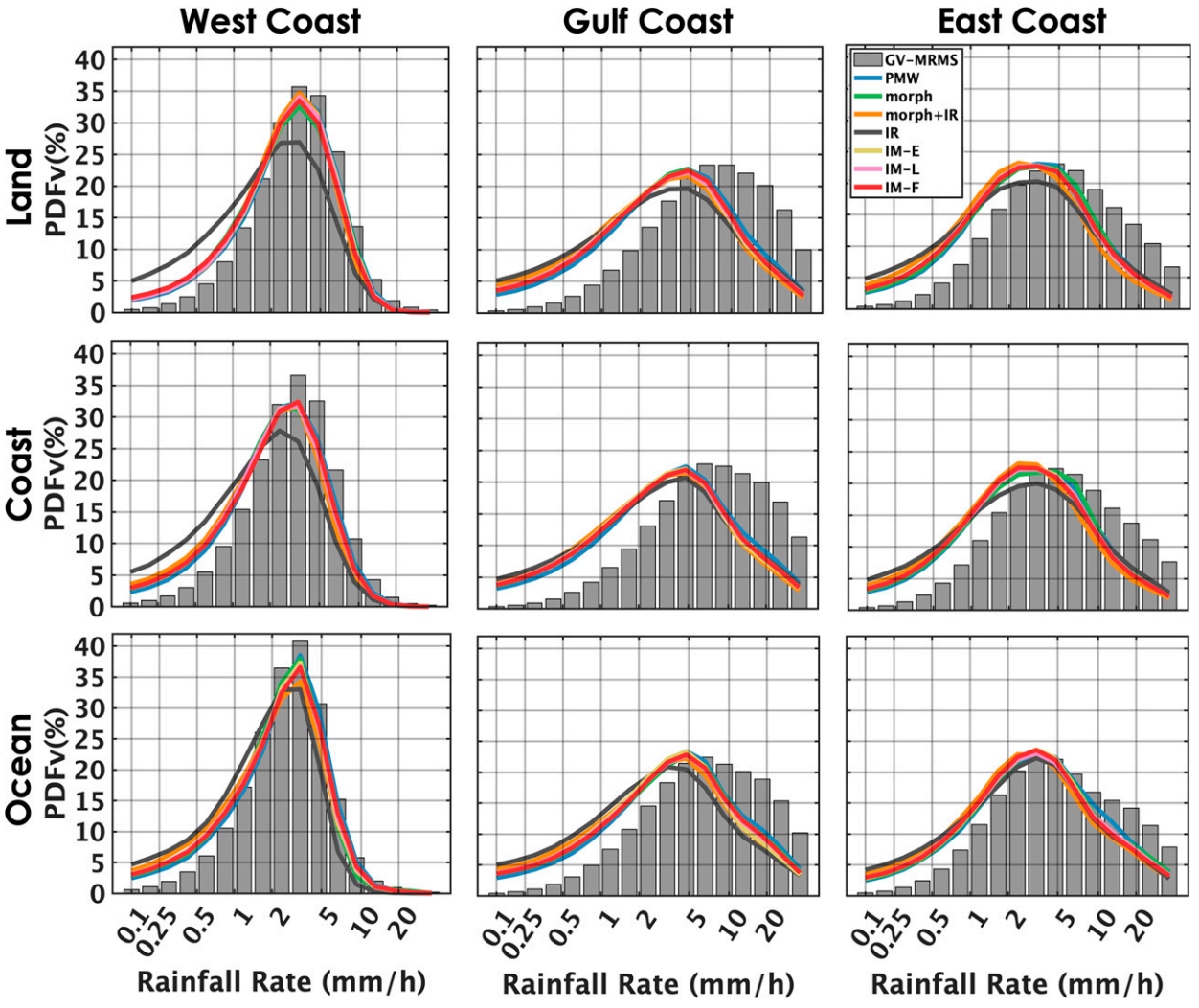

FIG. 4. PDF volume (PDF_v) as a function of GV-MRMS rainfall rate (mm h^{-1}) over the (left) West Coast, (center) Gulf Coast, and (right) East Coast regions and (top) land, (middle) coast, and (bottom) ocean surface types.

algorithms quantification challenges. Moreover, the Gulf Coast displays the lowest densities along the 1:1 line. Over the West Coast, IM-F is overestimating higher rainfall magnitudes for all surface types, with high density peaks above the 1:1 line. It is causing an overall overestimation (MRE values in the range [0.24–0.36]). Moreover, the lighter rainfall magnitudes tend to be underestimated by IM-F over all surface types over the West Coast region. IM-F quantification performance over the Gulf Coast is slightly different compared to other regions. The lighter rainfall magnitudes are overestimated over land and ocean surface types and underestimated over the coast surface type. Heavier rainfall magnitudes are overestimated for coast and ocean surface types and underestimated over the land surface type. IM-F quantification of lighter rainfall is similar over the East and the West Coast, with lighter rainfall is overestimated for all surface types.

IM-F quantification performance depends on surface types. Surprisingly in all regions the performance is lower over the ocean surface compared to coast and land surface types, with higher MRE and CRMSE.

b. *Performance based on distance from the coastline*

Figure 6 shows bivariate histograms of distance to the coastline as a function of GV-MRMS and IM-F matched rainfall over each region and surface type. For the sake of brevity, only the IM-F performance is presented. Perfect agreement between IM-F and GV-MRMS corresponds to the 1:1 line, while IM-F overestimation (underestimation) lays over (under) the 1:1 line. Each rainfall rate matched bin is colored by the mean distance to the coastline of the corresponding population of matched grids. Cold colors represent closer distances and warm colors represent further distances to the coastline. The perfect bivariate histogram of distance to coastline as a function of GV-MRMS and IM-F rainfall rates would gather all pairs on the 1:1 line with no cluster of colors. It should be noted that the sample size at the edges of this

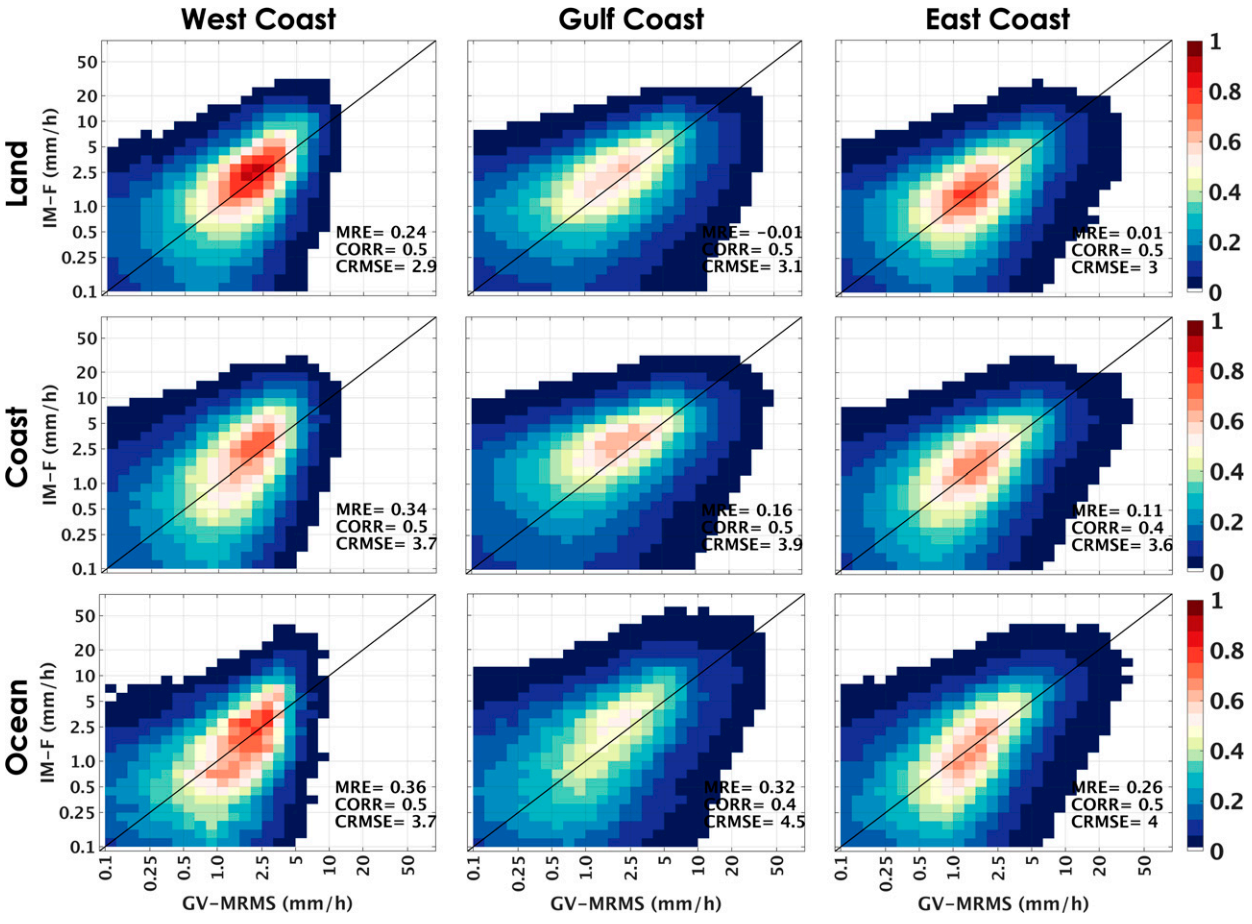

FIG. 5. Density scatter of IM-F and GV-MRMS (mm h^{-1}) over the (left) West Coast, (center) Gulf Coast, and (right) East Coast regions and (top) land, (middle) coast, and (bottom) ocean surface types. Each plot provides corresponding MRE, CRMSE and CORR.

plot is relatively smaller (see Fig. 5) and results in less robust statistics. This bivariate histogram helps us understand the performance of SPPs near the coastline over different surface types and regions.

Over the West Coast land surface type, lower IM-F and GV-MRMS rainfall magnitudes (<0.5 mm h^{-1}) are more often associated with larger distances to the coastline (range [90–110 km]), and they are slightly deviated from the 1:1 line (slight overestimation from IMERG). By contrast, higher rainfall magnitudes (>8 mm h^{-1}) are recorded by GV-MRMS closer to the coastline (within 75 km) that IM-F more often and significantly underestimates. Moisture-laden westerlies from the ocean generate high precipitation when they encounter the high mountain ranges of California, Oregon, and Washington (e.g., Olympic Mountains, Cascades, and Sierra Nevada range) while drier air generates less precipitation further inland. The IM-F underestimation closer to the coastline can be explained by the tenuous ice PMW scattering signatures generated by orographic warm rain processes. Also, IMERG may be challenged to estimate light precipitation over warm and heterogenous surfaces inland. Note an area of extreme GV-MRMS precipitation rates (>20 mm h^{-1}) at large distance (>100 km) that are underestimated by IM-F. Further analysis (not shown) indicates that this underestimation could relate to orographic precipitation in the Cascade Range located ~100 km away from the coastline. These trends and features are similar over the coastal surface, but gradients of distance with IM-F departures from the 1:1 line are more significant. IM-F overestimates GV-MRMS rainfall magnitudes 0.1–1.0 mm h^{-1} at distances far from the coastline. Underestimation at closer distance to the coastline is related to orographic precipitation that generates limited ice content aloft. The highest rates reported by both IM-F and GV-MRMS occur within 20 km of the coastline. They are associated with both significant underestimation (as already noted over land surface) and overestimation, which highlights the challenge for IMERG to estimate precipitation where emissivity gradients are mixed with orographic processes. Less dependance with distance is noted over ocean, but one can note a trend toward overestimation at large distances (>70 km) and for high rain rates (>5 mm h^{-1}).

Over the East Coast land and coastal surface types, there are three major clusters. In general, closer to the coastline, IMERG is overestimating and farther away from the coastline IMERG is underestimating significantly. Over the coastal surface type, IMERG substantially overestimates GV-MRMS

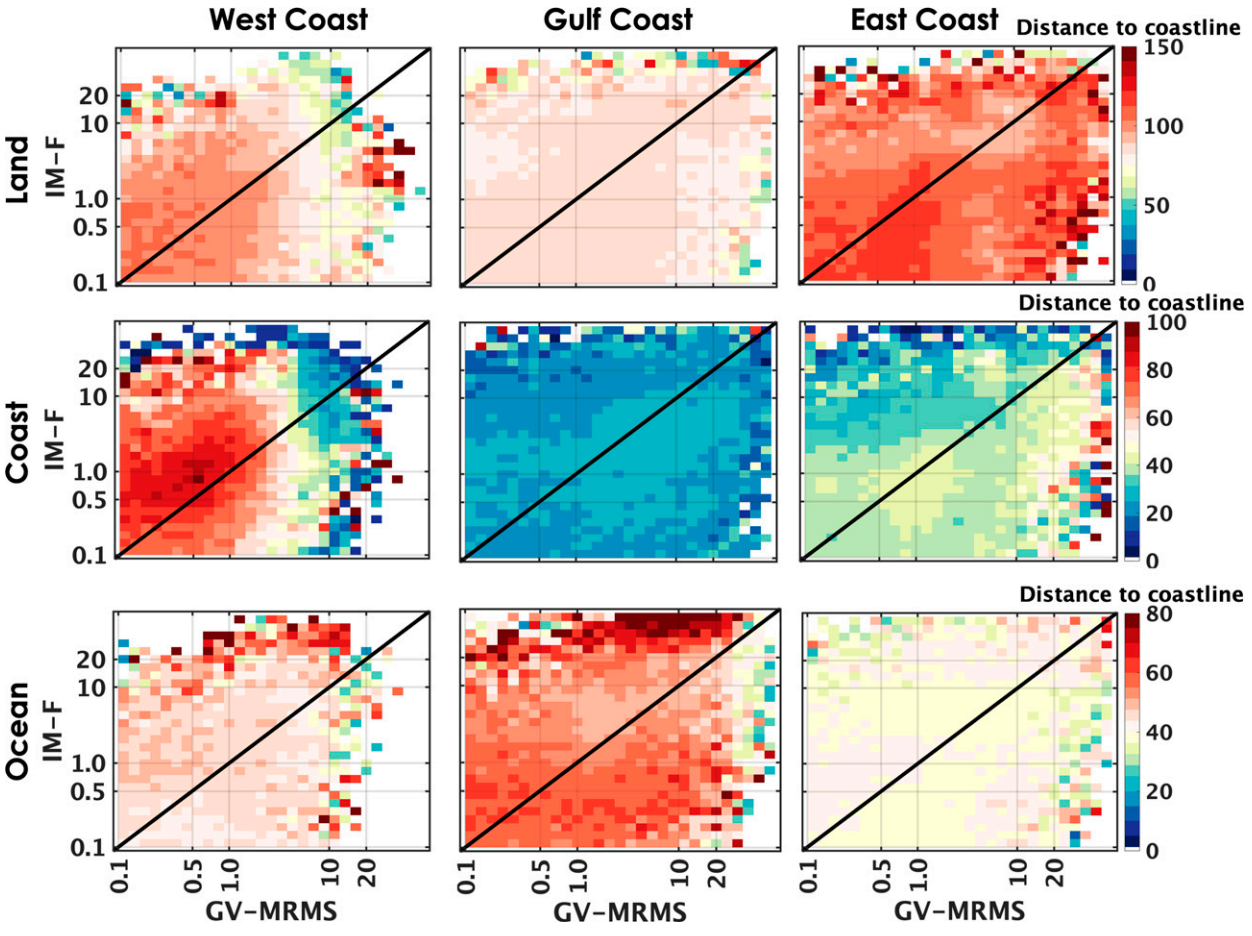

FIG. 6. Bivariate histogram of distance to coastline (km) as a function of GV-MRMS and IM-F rainfall (mm h^{-1}) over the (left) West Coast, (center) Gulf Coast, and (right) East Coast regions and (top) land, (middle) coast, and (bottom) ocean surface types. Note that the color bar limits for each surface type are different.

rainfall magnitudes in between 0.1 and 10 mm h^{-1} within ~20 km away from the coastline. IMERG starts to underestimate further away from the coastline at around ~50 km. Moreover, IMERG shows significant underestimation of GV-MRMS rainfall magnitudes greater than 20 mm h^{-1} farthest away from the coastline at around ~80 km. This change of quantification performance can be due to complex coastal features consisting of barrier islands and coastal inlets over this region and Appalachian Mountains farther away from the coastline.

Over the Gulf Coast, IMERG shows the least discrepancies as a function of distance from the coastline compared to other regions. IMERG shows similar performances over the land and coastal surface types, while over the ocean it has slightly different performance. Over the coastal surface type IMERG shows significant overestimation very close to the coastline. Meanwhile at around ~30 km away from the coastline IMERG performance is the best (near 1:1 line). Over the ocean surface IMERG in general significantly underestimates near the coastline and significantly overestimates far away from the coastline. At around ~50 km from the coastline the quantification performance of IMERG is better (near 1:1 line).

Gradients or clusters of distance with IM-F departures from the 1:1 line is less important in the Gulf and the East Coast regions. Overall, gradients tend to be more important over the coastal surfaces in all regions, and both Gulf and East coasts show large precipitation rate departures at the coastline, as expected. Over the ocean surface, a large underestimation is noted for high GV-MRMS rain rates (>10 mm h^{-1}) at closer distance to the coastline for all regions, consistent with the coastal features. The trend toward overestimation at large distances (>70 km) and for high rain rates (>5 mm h^{-1}) in the West Coast region is also noted in the Gulf, but not in the East Coast region. Over the land surface type, IM-F is overestimating GV-MRMS lower rainfall magnitudes. There is another cluster showing significant underestimation of heavier GV-MRMS rainfall magnitudes at farther distance from the coastline.

The distance to the coastline appears to have a large impact on IM-F quantification performance over the West Coast, and a slighter impact over the East Coast and the Gulf Coast. It confirms that the complex terrain proximity to the coastline over the West Coast has effects on IM-F quantification performance.

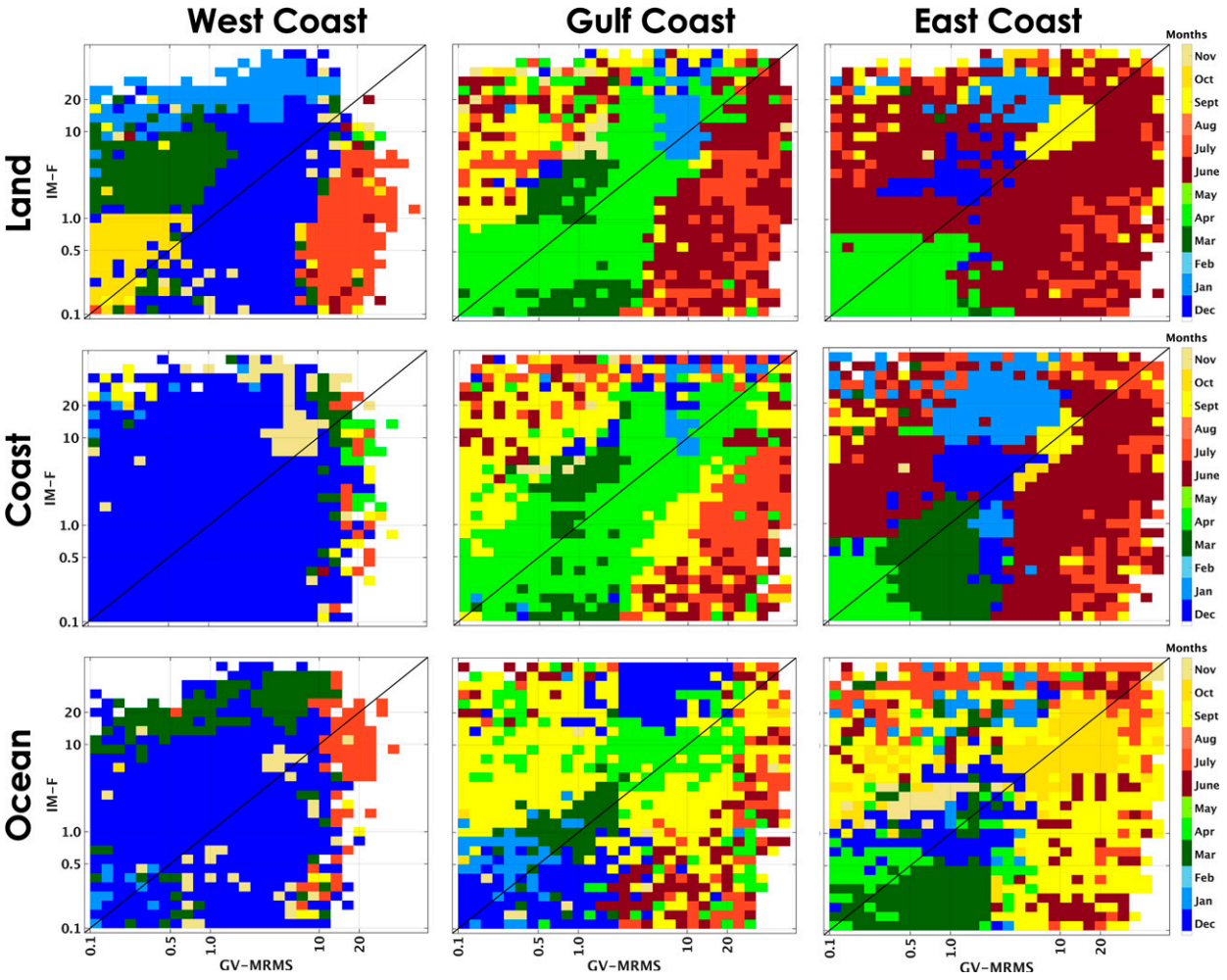

FIG. 7. Bivariate histogram of highest occurrence of months as a function of GV-MRMS and IM-F rainfall (mm h^{-1}) over the (left) West Coast, (center) Gulf Coast, and (right) East Coast regions and (top) land, (middle) coast, and (bottom) ocean surface types.

Similar to Fig. 6, Fig. 7 shows bivariate histograms of months of highest occurrence for GV-MRMS and IM-F matched rainfalls over each region and surface type. It should be noted that these two plots share the same GV-MRMS and IM-F rainfall magnitude bins. Hence, the same matched bins connect the distance to the coastline and the corresponding month of highest occurrence. Most of the matched pairs in the West Coast feature winter months (December and January) consistent with synoptic-scale cyclones and fronts from the Pacific Ocean that interact with coastal mountains. It generates high rain rates that are underestimated by IM-F, especially over the land surface type (Fig. 6). Over the coastal surface IM-F shows over and underestimation of all GV-MRMS rainfall magnitudes during winter months. Other high GV-MRMS rates underestimated by IM-F occur in August, especially over land at farther distance from the coastline (Fig. 6) in relation to orographic processes and the presence of a longwave ridge over most of the country during the late summer months. Overestimation of corresponding lighter rainfall magnitudes of GV-MRMS far away from the coastline (land and ocean) is observed during the September and March months.

The Gulf Coast displays more seasonal variations in the GV-MRMS-IM-F discrepancies. More agreement (close to 1:1 line) occurs in spring (March and April) especially over coastal and land surfaces. IM-F underestimation generally occurs during summer months, and overestimation tends to occur during fall months. It suggests that IM-F underestimates sea-breeze fronts, convective storms and tropical cyclones that are observed during the summer months. Meanwhile IM-F is overestimating the return flow of Gulf-modified warm, moist air and cold front passages during cooler seasons.

Over the East Coast, the clusters over land and coast surface types are quite similar to each other. Over the coast surface type, as mentioned in Fig. 6, IMERG largely overestimates the GV-MRMS rainfall magnitudes near the coastline and further away from the coastline IMERG overestimates substantially. This change in quantification performance is captured in Fig. 7 as well, during June, IMERG shows overestimation for lower GV-MRMS rainfall magnitudes and underestimation for

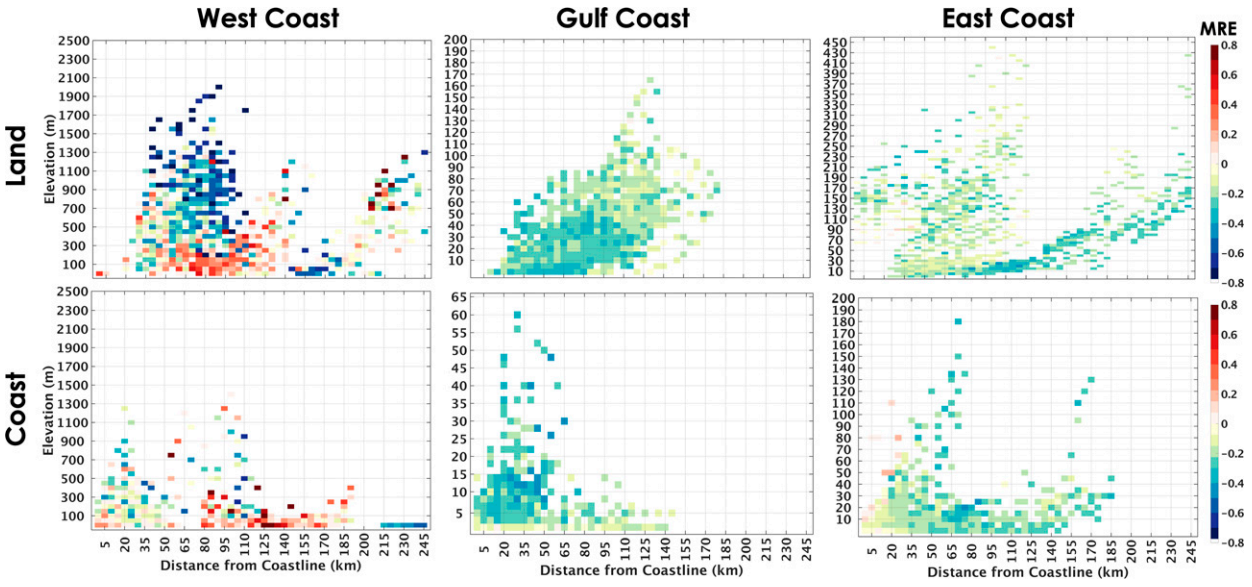

FIG. 8. Bivariate histogram of MRE as a function of distance from coastline (km) and elevation (m) over the (left) West Coast, (center) Gulf Coast, and (right) East Coast regions and (top) land and (bottom) coast surface types. Note that the *y*-axis limits for each subplot are different.

higher GV-MRMS rainfall magnitudes. Underestimation during June far away from the coastline is directly related to the complex terrain over the East Coast. Overestimation during June near the coastline can be related to the complex relations between atmosphere and coastal features consisting of barrier islands and coastal inlets. Moreover, at around ~50 km away from the coastline IMERG shows diverse performance (overestimation and underestimation) of GV-MRMS rainfall magnitudes in between 0.1 and 2 mm h^{-1}. It is clear from Fig. 7 that the overestimation of the GV-MRMS rainfall magnitudes by IMERG is observed over the June months meanwhile the underestimation is observed during the March months over the same regions. This shows that IMERG quantification performance is affected by the complex interactions between land–coast–ocean continuum during different seasons over the same locations.

IM-F large dependency on distance from the coastline over the West and East Coasts is further investigated with systematic departures conditioned on distance from the coastline and elevation. Figure 8 shows a bivariate histogram of MRE as a function of distance from the coastline (*x* axis; km) and with elevation (*y* axis; m) for each surface type and region. Each bin is colored by MRE value of IM-F against GV-MRMS, with warm colors for positive MRE (overestimation) and cold colors for negative MRE (underestimation).

In Fig. 8, over the West Coast land surface type IM-F biases strongly depend on elevation and distance to the coastline. Three main clusters of overestimation and underestimation can be separated. Their corresponding location at the West Coast is identified as they may reflect different meteorological patterns:

1) Cluster of an underestimation in the [35–110] km distance ranges from the coastline and at elevation higher than 300 m. This underestimation is located mainly in California near the coastline (not shown) which confirms that IM-F has low quantification performance of orographic rainfall.
2) Cluster of an overestimation within 145 km from the coastline and at elevation less than 450 m. This cluster is in Washington State and Oregon over the West Coast.
3) Cluster of mixed under/overestimation at distances greater than 155 km for elevations greater than 400 m. This cluster is in the north of Washington State. This diverse quantification performance of IM-F can be explained by a couple mechanisms. The first is IM-F underestimation of orographic enhancement where PMW has detection issues of warm clouds with lower ice content aloft. The second is IM-F overestimation, which can be explained by the lee side convergence (Kirshbaum et al. 2018) due to diurnal variability. The amount of observed rainfall is lower; however, IM-F is overestimating these mechanisms.

Similar features are noted over the West Coast coastal surface type.

Over the Gulf Coast, which is mainly characterized by flat terrain, both land and coast surface types display underestimation at all distances and terrain elevations. The underestimation is greater near the coastline and at lower elevations (MRE values in the range [−0.4 to 0.8]) than at larger distances from the coast (MRE values in between [0 and 0.2]). It confirms that the fundamental challenges when it comes to quantifying rainfall magnitudes over the land–coast–ocean transition zones in flat terrain as well.

Over the East Coast both land and coastal surface types display limited biases at all distances and terrain elevation. MRE values are within ±0.2 near the coastline, with more significant underestimation (MRE values in between [−0.4 and 0.8]) away from the coastline where complex terrain may trigger warm rain processes. As mentioned earlier on the East Coast

the Appalachian Mountains and other complex coastal features that include barrier islands and coastal inlets can generate either small overestimation or underestimation in IMERG. As mentioned in Fig. 7, overestimation near the coastline is observed over the summer months while underestimation near the coastline is observed over the winter months. Seasonal variations are driven by the Gulf Stream that conditions wind, humidity, and temperature patterns during the warm season, and by the occurrence of extratropical cyclones just offshore of the eastern CONUS during the cold season.

Figure 9 shows the bias dependence in terms of MRE with distance from the coastline for each SPPs. MRE values show significant dependence on distance from the coastline over land and coast surface types. In general, the highest overestimation is found with PMW [0.2–1.2] for almost all regions and surface types, while IM-F [−0.1 to 0.8] and IM-L [−0.2 to 1.1] show the lowest bias magnitudes.

As expected, the distance from the coastline exerts a more significant influence over the West Coast due to the large topography gradient adjacent to the ocean. Large overestimation occurs near the coastline over both land and coast surface types, which turns to lower overestimation at distances [10–20] km over land and [20–40] km over coast then back to significant overestimation further inland. As discussed earlier, IR performance differs from other SPPs, and its performance near the coastline is degraded with highest MRE [>0.8] values. Over the land surface type at 20 and 55 km from the coastline IR shows the lowest MRE [~0] values compared to other SPPs. IM-F has relatively lower MRE [0.1–0.4] values and PMW shows the highest MRE [0.2–1.0] values compared to other SPPs. PMW poor performance over this region can be inferred from orographic precipitation processes combined with coastal gradients of emissivity from ocean and land. Morphing has lower MRE [0.1–0.9] values compared to PMW. In Part I of this study, it was observed that morphing tends to increase the occurrence of lower retrieved rainfall rates. Over the coastal surface type, IM-F and PMW show the highest MRE [0.4–1.4] values while morph+IR, IR, and morph show the lowest MRE [0–0.8] values up to 65 km then beyond 65 km IR and IM-F show the lowest MRE [0.3–0.9] values. Over the ocean surface type, all SPPs show increasing overestimation with distance from the coastline while IR shows constant overestimation at +40%. Overall, IR MRE [~0.4] values display less dependance with distance from the coastline and overestimate at all distances. Other SPPs show slight underestimation near the coastline (except IM-F, PMW, morph, and IR show overestimation), which turns into an overestimation beyond 5 km offshore, with more dependance on the distance from the coastline. Morph+IR (PMW and IR) have the lowest (highest) MRE [−0.1 to 0.4] ([0.2–0.7]) values. IM-F and IM-L show slight differences in MRE up to 25 km away from the coastline while IM-L and IM-E performances are similar to each other. Beyond this distance IM-F, IM-L, and IM-E show very similar MRE values. The differences near the coastline can be attributed to the various IR and PMW contributions to the IMERG runs. PMW performance near the coast is the worst for all surface types and significantly influences IM-L and IM-E and propagates to IM-F.

Over the Gulf Coast, the dependence on the distance from the coastline is lowest compared to the other two regions, probably due to flatter terrain. One can note a shift toward higher MRE value from land to coast to ocean surfaces for all SPPs except IR. SPPs tend to overestimate at all distances from the coastline, with some exceptions. Again, PMW shows the highest overestimation [0.2–0.5] over all surface types. Over land, IM-F, and morph+IR show underestimation while other SPPs slightly overestimate. IM-L, IM-E, IR, and morph show similar and very low MRE [0–0.1] values. Surprisingly, even though morph and IR show similar MRE values (slight overestimation without dependence on distance from the coastline), morph+IR shows significantly different MRE [−0.1 to 0.1] (slight underestimation with dependence on distance from the coastline). This trend is reflected in IM-F because since the contribution of morph+IR to IM-F is the highest (see Fig. 2d showing the percentage contribution of morph+IR). Over the coast surface type, all SPPs except IM-F slightly overestimate GV-MRMS without dependence on distance from the coastline. In general, morph+IR and IM-F shows lower MRE values. Over ocean all SPPs overestimate GV-MRMS. IR and morph+IR show the lowest MRE values. IM-L, morph and IM-F show similar performances while IM-E has higher MRE values. As morph has higher contribution to IM-F over ocean in the Gulf Coast region (Fig. 2c), this is reflected in the IM-L and IM-F performances.

Over the East Coast, SPPs show slight overestimation with some exceptions, and again more significant overestimation over ocean. Over the land surface type IR and PMW have the highest MRE values while morph+IR and IM-F show the lowest MRE (close to zero). IR shows more significant dependence on distance; from the coastline, overestimation turns into slight underestimation farthest away from the coastline [−0.1 to 0.3]. IM-E, IM-L, and morph display similar MRE values (slight overestimation) with slight dependence on distance from the coastline. Over the coast surface type, SPPs MRE show the most dependence on distance from the coastline, especially the IR, IM-F, and morph+IR products. Beyond ~35 km away from the coastline, slight overestimation turns into underestimation, which might be related to barrier islands and coastal inlets or the warmer Gulf Stream. IM-F shows the highest underestimation [−0.1 to 0.1] while PMW shows the highest overestimation [0.2–0.3]. IM-E, IM-L, and morph products show the least dependence on distance from the coastline. Similar performance of IR and morph+IR over this surface type can be explained by the relatively higher contribution of IR (Fig. 2b) and IR uncertainty is carried over to morph+IR and eventually to IM-F. Over the ocean surface, SPPs show almost no dependance on distance from the coastline compared to the other surface types. PMW shows the highest overestimation, followed by IM-E and IM-F, and morph+IR and IR have the lowest MRE.

c. *Precipitation typology*

As typology is a key characteristic of precipitation (Kirstetter et al. 2020), IMERG quantification performance is investigated as a function of precipitation types, i.e., GV-MRMS stratiform

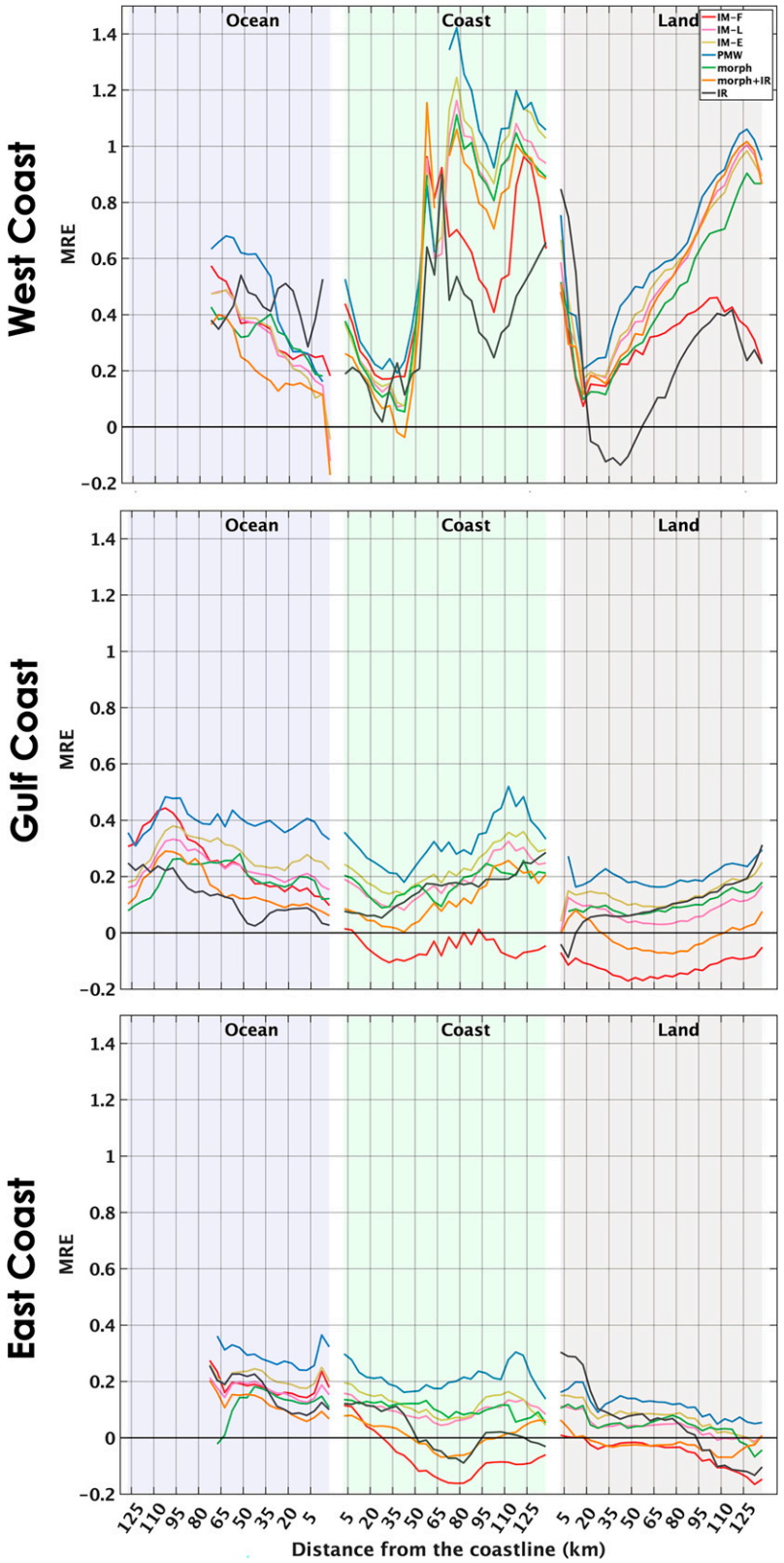

FIG. 9. MRE as a function of distance from coastline over the (left) West Coast, (center) Gulf Coast, and (right) East Coast regions and (top) land, (middle) coast, and (bottom) ocean surface types for all SPPs.

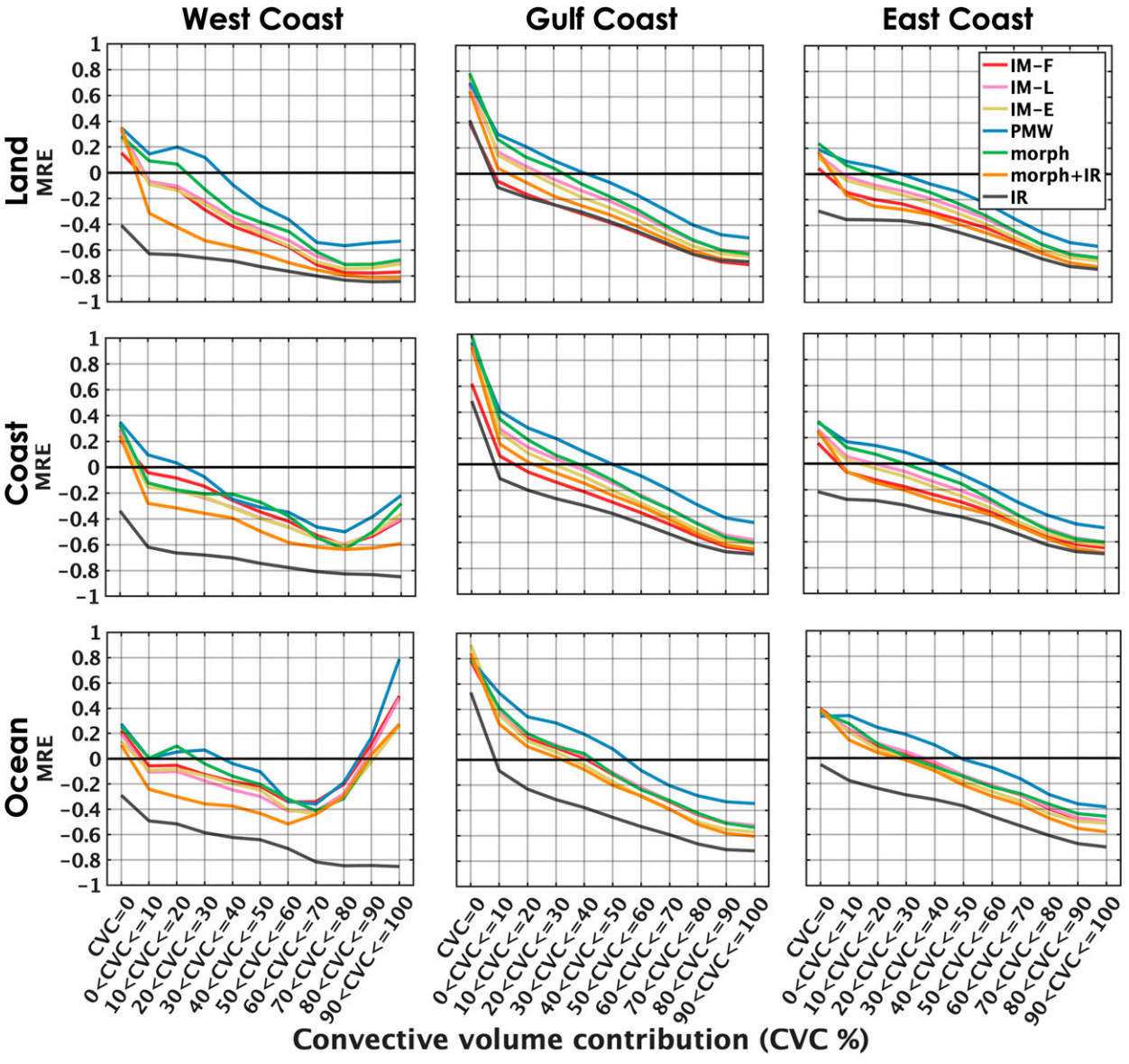

FIG. 10. MRE as a function of convective volume contribution over the (left) West Coast, (center) Gulf Coast, and (right) East Coast regions and (top) land, (middle) coast, and (bottom) ocean surface types for all SPP.

vand convective rainfall. Any pixel with positive convective volume contribution is a convective case meanwhile any pixel with zero convective volume contribution is a stratiform case. Figure 10 provides MRE for each product, over each surface type, and region for stratiform and convective precipitation types. Overall, SPPs (with IR exceptions) show overestimation for stratiform rainfall (MRE in the range [0–0.8]) and increasing underestimation for more convective precipitation (up to −0.8). Only over the West Coast ocean surface type SPPs significantly overestimate convective precipitation. Over all regions and surface types, PMW shows overestimation of stratiform cases (MRE in the range [0.2–0.8]) meanwhile shows over/underestimation of convective cases (MRE in the range [−0.5 to 0.6]). IR, on the other hand, shows over/underestimation of stratiform cases (MRE in the range [−0.4 to 0.4]) and meanwhile shows significant underestimation of convective cases (MRE in the range [−0.8 to −0.7]).

Over the West Coast region SPPs performance vary over each surface type, which reflects the varying precipitation processes and their SPP retrieval. Over the land surface type, all SPP MREs show a dependence on precipitation type with slight overestimation of stratiform precipitation rates (except IR) and underestimation of convective rates. The effects of each sensor and product type on IM-F, IM-L, and IM-E are very clear. Morph and PMW MRE [−0.6 to 0.4] performances are close to each other with lowest MRE values. Meanwhile IR and morph+IR performances [−0.8 to 0.2] are also similar to each other with highest MRE values. IM-F, IM-E, and IM-L

MRE values lie in between these two groups. Over coast surface, IR has the lowest MRE [−0.8 to −0.4] values and stand out with respect to the other SPPs. SPP underestimations are smaller for the convective precipitation type compared to over land surface. This could be due to more prevalent warm rain processes in the mountains compared to the coast. Over the ocean surface type, SPPs surprisingly overestimate rates associated with higher convective volume contribution except IR. Similar to other two surface types, IM-F, IM-L, IM-E, and morph MRE values lay in between PMW [−0.3 to 0.8] and morph+IR [−0.5 to 0.3] MRE values.

Over the Gulf Coast, all SPPs show similar MRE values for all surface types. All SPPs show decreasing MRE values with convective volume contribution, (PMW [−0.5 to 0.8] and IR [−0.7 to 0.4] MRE values). Over the land and coast surface types, IM-F MRE values are similar to IR and morph+IR, while over ocean IM-F and morph MRE values are more similar.

Similar trends can be seen over the East Coast, with some differences. The overestimation of stratiform precipitation is less important than in the Gulf Coast. IR underestimates [−0.7 to 0.1] GV-MRMS rainfall magnitudes for all convective contributions. Again, over the land and coast surface type IM-F and morph+IR MRE [−0.7 to 0.4] values are similar to each other; IM-L and IM-E MRE values are similar to each other and slightly lower compared to IM-F MRE values. Over the ocean surface type, all SPPs show very similar MRE values [−0.6 to 0.4] and lay between PMW and IR.

4. Conclusions

The ability to quantify rainfall over the land–coast–ocean continuum is examined over three coastal regions of the United States, i.e., the West Coast, Gulf of Mexico, and East Coast. Each region is characterized by different topographies and precipitation climatologies. Complementing Part I of this analysis on the detection capabilities of IMERG, quantification performances are examined over the land–coast–ocean continuum. Specifically, the quantification performance of each SPP is examined by distance from the coastline and the corresponding elevation to understand the impact of complex terrain proximity to the coastline on SPP quantification performance. The influence of stratiform and convective rainfall is also examined. An integrated and novel approach is developed to trace the quantification performance of IMERGV06B (IM-F, IM-L, IM-E) back to their components (PMW, morph, morph+IR, and IR) and sources of rainfall estimates.

The main results are summarized as follows:

- Level-3 IM-F quantification performance heavily depends on the respective contribution of PMW, IR-only, morph, and morph+IR components. IMERG components have spatially uneven contributions to the merged products.
- IM-F and its components in general have similar PDF_c distributions compared to the GV-MRMS except IR. However, SPPs PDF_v distributions show systematic characteristics and departures with respect to GV-MRMS. SPPs PDF_v overestimate the contribution of light rainfall (<1 mm h^{-1}) and underestimate the contribution of high rainfall rates (>3 mm h^{-1}) to the total rainfall volume, indicating that IM-F and its components meet challenges in quantification of extreme precipitation events. This challenge was also reported by Tian et al. (2018) and Xu et al. (2017). Decreasing quantification performances are consistently noted with retrievals that rely on observations more indirectly related to surface precipitation. Overall, IMERG displays nonhomogeneous precipitation quantification properties that vary according to which component is used, and that translates into nonhomogeneous accuracy in space and time.
- IM-F and IM-L performances of quantification of rainfall are very similar to each other where IM-L has slightly higher CRMSE values compared to IM-F, suggesting that the monthly gauge correction does not influence the quantity of precipitation across IM-L and IM-F products. It could be due to lack of reporting rain gauges over land–coast–ocean continuum or monthly rain gauge adjustment technique is not sufficient to improve performance of IM-L.

Part I highlighted the positive impact of morphing on precipitation detection. Morph showed highest discrimination ability with respect to GV-MRMS up to ~2 mm h^{-1} threshold, and above this threshold PMW showed the highest discrimination skill. When it comes to quantification, PMW displays lower magnitudes of systematic and random error compared to morph. Each IMERG product's performance depends on location because rainfall characteristics and their spatial distributions vary across the United States.

- Each region has distinct precipitation regimes and characteristics that are captured by SPPs with varying accuracy. Each IMERG product and component shows variations in quantification performance that highlight the impact of terrain and climatology.
- The proximity of complex terrain to the coastline in the West Coast is particularly challenging. Moisture-laden westerlies from the ocean generate high precipitation when they encounter the high mountain ranges of California, Oregon, and Washington (e.g., Olympic Mountains, Cascades, and Sierra Nevada range) while drier air generates less precipitation further inland. Higher rainfall magnitudes (>8 mm h^{-1}) are recorded by GV-MRMS closer to the coastline (within 75 km) that IM-F more often and significantly underestimates. This can be explained by the tenuous ice PMW scattering signatures generated by orographic warm rain processes. Also, IMERG may be challenged to estimate light precipitation over warm and heterogenous surfaces inland.
- Over the East Coast, quantification performance of IMERG over North Carolina, Virginia, and the Long Island barrier islands and coastal inlets shows seasonal dependence. Over the coastal surface type, IMERG overestimates during the summer months and underestimates during the winter months. Surface types have a considerable influence that is attributed to emissivity gradients and contrasts in land/ocean precipitation characteristics.

IMERG products and its components show significant dependence on distance from the coastline and elevation, especially over the land and coast surface types.

- Distance to the coastline dependence tends to be more important over the coastal surfaces compared to other surface types. All regions show large precipitation rate departures at the coastline.
- Distance to the coastline dependence tend to be less important over the ocean surface type but one can note a trend toward an overestimation at large distance from the coastline for high rain rates (>5 mm h^{-1}).

Regional differences (especially the West Coast) result from precipitation processes and generation mechanisms that are not captured by IMERG. This is highlighted with the impact of precipitation typology.

- Overall IMERG products and components show significant different rainfall quantification performances for convective and stratiform rainfall. In general, SPPs (with exception of IR) show slight to significant overestimation for stratiform rainfall type, meanwhile products show significant underestimation for convective rainfall type (the West Coast ocean surface type excluded).
- Depending on the percentage occurrence of each component used to create IM-F, IM-F performance of quantifying rainfall type changes. For example, over the West Coast IM-F performance is similar to morph since the percentage of occurrence of morph is higher over this region. In an analogous manner, over the Gulf Coast morph+IR has the highest percentage occurrence hence IM-F and morph+IR performance of quantifying rainfall type is very similar to each other.
- Quantification of stratiform and convective rainfall magnitudes vary slightly across regions, which highlights the impact of precipitation regimes.

Overall, orographic rainfall mechanisms and precipitation type have the biggest influences on error characteristics of SPPs relative to the land–coast–ocean differences. As precipitation typology is a strong characteristic that is currently not accounted for in IMERG, these results call for ingesting the GPROF precipitation type information into IMERG. It would potentially increase IMERG accuracy and its consistency across regions. As future directions of this study, SPP performances over CONUS complex terrain will be investigated along with the influence of environmental variables.

Acknowledgments. The authors would like to acknowledge the efforts made by the NASA science team for making IMERG precipitation data accessible. Support from the NASA Global Precipitation Measurement Ground Validation program under Grant NNX16AL23G and the Precipitation Measurement Missions program under Grant 80NSSC21K2045 are acknowledged.

Data availability statement. The GV-MRMS precipitation data are available at the NASA Global Hydrology Resource Center (GHRC) (http://dx.doi.org/10.5067/GPMGV/MRMS/DATA101). The IMERG precipitation products can be downloaded at https://arthurhouhttps.pps.eosdis.nasa.gov.

REFERENCES

Carr, N., and Coauthors, 2015: The influence of surface and precipitation characteristics on TRMM Microwave Imager rainfall retrieval uncertainty. *J. Hydrometeor.*, **16**, 1596–1614, https://doi.org/10.1175/JHM-D-14-0194.1.

Derin, Y., P. E. Kirstetter, and J. J. Gourley, 2021: Evaluation of IMERG satellite precipitation over the land–coast–ocean continuum. Part I: Detection. *J. Hydrometeor.*, **22**, 2843–2859, https://doi.org/10.1175/JHM-D-21-0058.1.

Gebregiorgis, A. S., P. Kirstetter, Y. E. Hong, N. J. Carr, J. J. Gourley, W. Petersen, and Y. Zheng, 2017: Understanding overland multisensor satellite precipitation error in TMPA-RT products. *J. Hydrometeor.*, **18**, 285–306, https://doi.org/10.1175/JHM-D-15-0207.1.

——, and Coauthors, 2018: To what extent is the day 1 GPM IMERG satellite precipitation estimate improved as compared to TRMM TMPA-RT? *J. Geophys. Res. Atmos.*, **123**, 1694–1707, https://doi.org/10.1002/2017JD027606.

Hou, A. Y., and Coauthors, 2014: The Global Precipitation Measurement mission. *Bull. Amer. Meteor. Soc.*, **95**, 701–722, https://doi.org/10.1175/BAMS-D-13-00164.1.

Houze, R. A., Jr., 2012: Orographic effects on precipitating clouds. *Rev. Geophys.*, **50**, RG1001, https://doi.org/10.1029/2011RG000365.

Huffman, G. J., and Coauthors, 2019: NASA Global Precipitation Measurement (GPM) Integrated Multi-satellitE Retrievals for GPM (IMERG). Algorithm Theoretical Basis Doc., version 6, 34 pp., https://gpm.nasa.gov/sites/default/files/document_files/IMERG_ATBD_V06.pdf.

——, and Coauthors, 2020: Integrated Multi-satellite Retrievals for the Global Precipitation Measurement (GPM) Mission (IMERG). *Satellite Precipitation Measurement*, V. Levizzani, eds, Advances in Global Change Research, Vol. 67, Springer, 343–353, https://doi.org/10.1007/978-3-030-24568-9_19.

Kirshbaum, D. J., B. Adler, N. Kalthoff, C. Barthlott, and S. Serafin, 2018: Moist orographic convection: Physical mechanism and links to surface-exchange process. *Atmosphere*, **9**, 80, https://doi.org/10.3390/atmos9030080.

Kirstetter, P.-E., and Coauthors, 2012: Toward a framework for systematic error modeling of spaceborne precipitation radar with NOAA/NSSL ground radar-based National Mosaic QPE. *J. Hydrometeor.*, **13**, 1285–1300, https://doi.org/10.1175/JHM-D-11-0139.1.

——, Y. Hong, J. J. Gourley, Q. Cao, M. Schwaller, and W. Petersen, 2014: A research framework to bridge from the Global Precipitation Measurement mission core satellite to the constellation sensors using ground radar-based National Mosaic QPE. *Remote Sensing of the Terrestrial Water Cycle, Geophys. Monogr.*, Vol. 206, Amer. Geophys. Union, 61–79.

——, ——, ——, M. Schwaller, W. Petersen, and Q. Cao, 2015: Impact of sub-pixel rainfall variability on spaceborne precipitation estimation: Evaluating the TRMM 2A25 product. *Quart. J. Roy. Meteor. Soc.*, **141**, 953–966, https://doi.org/10.1002/qj.2416.

——, N. Karbalaee, K. Hsu, and Y. Hong, 2018: Probabilistic precipitation rate estimates with space-based infrared sensors.

Quart. J. Roy. Meteor. Soc., **144**, 191–205, https://doi.org/10.1002/qj.3243.

——, W. A. Petersen, C. D. Kummerow, and D. B. Wolff, 2020: Integrated multi-satellite evaluation for the Global Precipitation Measurement mission: Impact of precipitation types on spaceborne precipitation estimation. *Satellite Precipitation Measurement*, Vol. 2, V. Levizzani et al., Eds., Advances in Global Change Research, Vol. 69, Springer, 583–608, https://doi.org/10.1007/978-3-030-35798-6_7.

Kummerow, C. D., 2020: Introduction to passive microwave retrieval methods. *Satellite Precipitation Measurement*, Vol. 1, V. Levizzani et al., Eds., Advances in Global Change Research, Vol. 67, Springer, 123–140, https://doi.org/10.1007/978-3-030-24568-9_7.

——, and L. Giglio, 1994: A passive microwave technique for estimating rainfall and vertical structure information from space. Part I: Algorithm description. *J. Appl. Meteor. Climatol.*, **33**, 3–18, https://doi.org/10.1175/1520-0450(1994)033<0003:APMTFE>2.0.CO;2.

——, and Coauthors, 2001: The evolution of the Goddard profiling algorithm (GPROF) for rainfall estimation from passive microwave sensors. *J. Appl. Meteor.*, **40**, 1801–1820, https://doi.org/10.1175/1520-0450(2001)040%3C1801:TEOTGP%3E2.0.CO;2.

Nalbantis, I., 2008: Evaluation of a hydrological drought index. *Eur. Water*, **23**, 67–77.

National Weather Service, 2018: August/September 2017 Hurricane Harvey. NWS Service Assessment, 78 pp., https://www.weather.gov/media/publications/assessments/harvey6-18.pdf.

Prigent, C., W. B. Rossow, and E. Matthews, 1997: Microwave land surface emissivities estimated from SSM/I observations. *J. Geophys. Res.*, **102**, 21 867–21 890, https://doi.org/10.1029/97JD01360.

Purnell, D. J., and D. J. Kirshbaum, 2018: Synoptic control over orographic precipitation distributions during the Olympics Mountains Experiment (OLYMPEX). *Mon. Wea. Rev.*, **146**, 1023–1044, https://doi.org/10.1175/MWR-D-17-0267.1.

Rappaport, E. N., 2014: Fatalities in the United States from Atlantic tropical cyclones: New data and Interpretation. *Bull. Amer. Meteor. Soc.*, **95**, 341–346, https://doi.org/10.1175/BAMS-D-12-00074.1.

Roe, G. H., 2005: Orographic precipitation. *Annu. Rev. Earth Planet. Sci.*, **33**, 645–671, https://doi.org/10.1146/annurev.earth.33.092203.122541.

Sui, X., Z. Li, Z. Ma, J. Xu, S. Zhu, and H. Liu, 2020: Ground validation and error sources identification for GPM IMERG product over the southeast coastal regions of China. *Remote Sens.*, **12**, 4154, https://doi.org/10.3390/rs12244154.

Tan, J., W. A. Petersen, and A. Tokay, 2016: A novel approach to identify sources of errors in IMERG for GPM ground validation. *J. Hydrometeor.*, **17**, 2477–2491, https://doi.org/10.1175/JHM-D-16-0079.1.

Tian, F., S. Hou, L. Yang, H. Hu, and A. Hou, 2018: How does the evaluation of the GPM IMERG rainfall product depend on gauge density and rainfall intensity? *J. Hydrometeor.*, **19**, 339–349, https://doi.org/10.1175/JHM-D-17-0161.1.

Turk, F. J., and Coauthors, 2021: Adapting passive microwave-based precipitation algorithms to variable microwave land surface emissivity to improve precipitation estimation from the GPM constellation. *J. Hydrometeor.*, **22**, 1755–1781, https://doi.org/10.1175/JHM-D-20-0296.1.

Wang, D., X. Wang, L. Liu, D. Wang, H. Huang, and C. Pan, 2019: Evaluation of TMPA 3B42V7, GPM IMERG and CMORPH precipitation estimates in Guangdong Province, China. *Int. J. Climatol.*, **39**, 738–755, https://doi.org/10.1002/joc.5839.

Wang, J., W. A. Petersen, and D. B. Wolff, 2021: Validation of satellite-based precipitation products from TRMM to GPM. *Remote Sens.*, **13**, 1745, https://doi.org/10.3390/rs13091745.

Wang, N.-Y., C. Liu, R. Ferraro, D. Wolff, E. Zipser, and C. Kummerow, 2009: TRMM 2A12 land precipitation product-status and future plans. *J. Meteor. Soc. Japan*, **87A**, 237–253, https://doi.org/10.2151/jmsj.87A.237.

Wolff, D. B., and B. L. Fisher, 2008: Comparisons of instantaneous TRMM ground validation and satellite rain-rate estimates at different spatial scales. *J. Appl. Meteor. Climatol.*, **47**, 2215–2237, https://doi.org/10.1175/2008JAMC1875.1.

Xu, W., S. A. Rutledge, and W. Zhang, 2017: Relationships between total lightning, deep convection, and tropical cyclone intensity change. *J. Geophys. Res. Atmos.*, **122**, 7047–7063, https://doi.org/10.1002/2017JD027072.

Yilmaz, K. K., T. S. Hogue, K. L. Hsu, S. Sorooshian, H. V. Gupta, and T. Wagener, 2005: Intercomparison of rain gauge, radar, and satellite-based precipitation estimates with emphasis on hydrologic forecasting. *J. Hydrometeor.*, **6**, 497–517, https://doi.org/10.1175/JHM431.1.

Young, G. S., and T. D. Sikora, 2003: Mesoscale stratocumulus bands caused by Gulf Stream meanders. *Mon. Wea. Rev.*, **131**, 2177–2191, https://doi.org/10.1175/1520-0493(2003)131<2177:MSBCBG>2.0.CO;2.

Zhang, J., Y. Qi, C. Langston, and B. Kaney, 2011: Radar quality index (RQI) – A combined measure of beam blockage and VPR effects in a national network. *IAHS Publ.*, **351**, 388–393.